

Automated Thermal Coagulation Segmentation of Three-Dimensional Elastographic Imaging using an Active Contour Model

Wu Liu¹, J.A. Zagzebski^{1,2}, T. Varghese^{1,3}, C.R. Dyer⁴, and U. Techavipoo^{1,5}

¹Department of Medical Physics

²Department of Radiology

³Department of biomedical Engineering,

⁴Department of Computer Sciences

⁵Department of Electrical and Computer Engineering

University of Wisconsin-Madison

Madison, WI, USA

Email: wuliu@wisc.edu

Abstract—Delineation of RF-ablator induced coagulation (thermal lesion) boundaries is an important clinical problem not well addressed by conventional imaging modalities. Automation of this process is certainly desirable. Elastography that estimates and images the local strain corresponding to small, externally applied, quasi-static compressions can be used for visualization of thermal coagulations. Several studies have demonstrated that coagulation volumes computed from multiple planar slices through the region of interest are more accurate than volumes estimated assuming simple shapes and incorporating single or orthogonal diameter estimates. This paper presents an automated segmentation approach for thermal coagulations on three-dimensional elastographic data to obtain both area and volume information. This approach consists of a coarse-to-fine method for active contour initialization and a gradient vector flow active contour model for deformable contour optimization with the help of prior knowledge of the geometry of general thermal coagulations. The performance of the proposed algorithm is shown to be comparable to manual delineation by medical physicists ($r = 0.99$ for 36 RF-induced coagulations). The correlation coefficient of the coagulation volume between auto-segmented elastography and manually-delineated pathology is 0.96.

Keywords—*elastography, image analysis, radiofrequency ablation, segmentation, strain, ultrasound*

I. INTRODUCTION

Radiofrequency (RF) tumor ablation has provided an effective and safe means to treat a large variety of benign and malignant conditions and holds promise as a treatment on an outpatient basis [1-3]. RF Ablation is an interstitial focal ablative therapy in which an electrode is placed into a tumor to cause heating and cauterization of the tumor from ionic agitation. The rapid vibration of ions creates friction, therefore, heating of the region of interest.

Imaging modalities that dynamically monitor the irreversible cellular damage evolution during and after

treatment are important to the success of RF ablation therapy [1, 2]. Ablative therapy is usually guided by Ultrasound and CT. However, CT is not suitable for real-time monitoring and coagulation to tissue-background contrast is poor on B-mode images. RF ablation is known to cause increases in the stiffness of tissue at the treated site. Elastography [4, 5] detects and images the local strain corresponding to a small, externally applied quasi-static compression. Local tissue displacements are estimated using a normalized time-domain cross-correlation between gated pre- and post-compression US radiofrequency echo signals. The gradient of the tissue displacement in the axial direction provides an estimate of local tissue strain. Elastography is sensitive to small changes in elastic modulus [6], and thus, it has the potential to image and differentiate the thermal coagulation necrosis from normal surrounding tissue. Three-dimensional (3D) images such as with multiplanar reconstruction, shaded surface processing, or volumetric processing, provides more meaningful representations of the underlying data set than planar images alone [7]. We have shown that 3D US elastography exhibits high coagulation-to-liver contrast, good correlation with pathology, and performs better than conventional US and CT [8-10].

Elastography is a promising tool for 3D visualization of RF ablation therapy thermal coagulations. However, manual delineation of boundaries on multiple planar two-dimensional (2D) images is tedious and labor intensive. Automatic extraction of lesion boundaries would be attractive to remove possible subjectivity and reduce assessment time. Although automatic and semiautomatic segmentation has been described for other imaging modalities, it has not been well addressed for elastographic depiction of structures. Two methods have been reported in the literature for automatic segmentation of elastographically delineated boundaries: (1) a simple threshold method [11] to segment lesion/tissue-background for semi-automated segmentation of regions treated by high-intensity focused ultrasound and (2) our previous semi-automated algorithm [12] for delineating RF-induced thermal coagulations

This work was supported in part by Whitaker Foundation grant RG-02-0457, start-up funds awarded to Dr. Varghese by the University of Wisconsin-Madison, and by NIH grant R21-EB002722.

on elastograms, which is based on thresholding and morphologic operations.

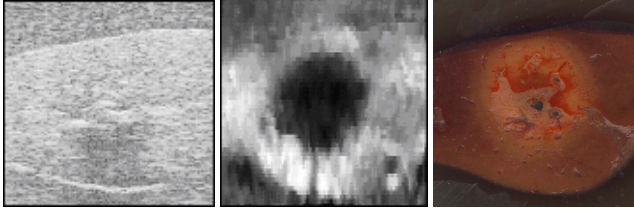


Figure 1. Ultrasonic (left), elastographic (center), and pathological (right) views of a typical thermal coagulation.

Figure 1 shows ultrasonic, elastographic, and pathological views of one slice of a typical thermal coagulation. The elastographic image has been pre-processed by using several image enhancement techniques. The purpose of the work described in this paper is to propose a fully automated method to segment the stiff lesion (the central darker circular area) from the background in 2D and 3D elastograms. Segmented regions would be used for measuring cross-sectional areas and volumes. The proposed algorithm is based on a coarse-to-fine method [13] for active contour initialization and a gradient vector flow active contour model [14] for deformable contour optimization with the help of prior knowledge of the geometry of general thermal coagulations.

II. MATERIAL AND METHODS

A. Data Acquisition

RF ablation *in vitro* was performed on specimens of freshly excised canine liver tissue having approximate dimensions of 40mm by 30mm, and 25 – 40mm thickness. A RITA model 460kHz 1500 RF generator (RITA Medical System, Mountain View, CA, USA) with nine StarBurst XL multi-tined expandable electrodes was used for the ablation procedures. The electrode consisted of a 15cm long 14-gauge stainless steel shaft insulated to within 1cm of the tip by a thin plastic layer, through which 9 sharp tines (0.53mm in diameter) can be deployed or retracted manually. The electrode was inserted into a liver specimen, and the tines were carefully deployed to provide 2-3cm active lengths in addition to the 1cm active tip of the shaft. The tines were deployed in an "umbrella" configuration at 45-degree intervals, along with the central tine. A foil ground pad was attached to the bottom surface of the liver specimen. RF ablation of the target tissue was performed at a 150-watt power level setting for 10min duration after different target temperatures (70°, 80°, 90°, and 100°C) were reached to create coagulations with different volumes. Forty-four RF coagulations were created, scanned, and measured to obtain the thermal coagulation area and volume. After the ablated liver specimen had cooled to room temperature, it (along with the RF electrode, for inscribing fiducial markers) was encased in a gelatin block, 110mm by 80mm and 70mm thickness, for subsequent imaging.

On the second day after the procedure, the gelatin block containing a liver specimen was removed from the mold and placed in an apparatus for elastographic imaging at room

temperature. An Aloka SSD 2000 (Aloka, Tokyo, Japan) real-time ultrasound scanner with a 42 mm 5-MHz linear array transducer with a 70% bandwidth was used. By manually translating the gelatin block parallel to the scan plane and repeating the data acquisition steps for each plane, 3D elastographic data were acquired. A 2mm distance between planes (the elevational resolution is slightly larger than 2mm) was precisely controlled using a precision linear stage. In general, about 20 slices were acquired for each phantom and among them about 15 slices contained the thermal coagulation.

Time-domain cross-correlation analysis of RF echo signals from the pre- and post-compression data sets (0.5% compression) was performed using a window length of 3mm with a 75% overlap between data segments to compute tissue displacements. Axial strain was estimated using a least squares strain estimator [15] with a kernel size of 2.25mm.

After ultrasound scans, the liver specimens were fixed by formalin solution for at least 2 weeks and then sliced in 2mm intervals. The tissue slices were placed on a transparent film and photographically scanned. These fixed gross-pathology images were used to obtain volume estimations of the thermal coagulation.

B. 2D/3D Segmentation

The active contour algorithm (aka snakes) is a well-known technique for detecting an object's boundary [16, 17]. A snake is defined as an energy-minimizing spline. The snake's energy depends on its shape and location within the image. In constructing a contour of an object's boundary, generally, we first place an initial spline (snake) on the image, and then its energy is minimized through spline deformation. Local minima of this energy correspond to desired image properties. The snake is defined parametrically as $X(s)=[x(s),y(s)]$, where $s \in [0,1]$ is the normalized arc length along the contour. The energy functional to be minimized may be written as

$$E_{total}^* = \int_0^1 E(X(s))ds = \int_0^1 E_{int}(X(s))ds + \int_0^1 E_{image}(X(s))ds + \int_0^1 E_{con}(X(s))ds$$

where E_{int} is the internal energy of the snake due to bending, E_{image} measures image forces, and E_{con} describes external constraint forces. The internal spline energy can be written as:

$$E_{int} = \alpha(s)|dX/ds|^2 + \beta(s)|d^2X/d^2s|^2$$

where $\alpha(s)$ and $\beta(s)$ specify the "elasticity" and "stiffness" of the snake, respectively. The image forces, $E_{image} \psi$ are derived from the image data over which the snake lies. Three important features that a snake can be attracted to are line, edge, and endpoint functions. The total image energy can be expressed as a weighted combination of these three features. Gradient vector flow (GVF) defines an external force (see reference [14] for details). It improves the performance of conventional snakes because GVF active contours have a larger capture range, i.e., are less sensitive to contour initialization, and exhibits better convergence to boundary concavities.

Although GVF snakes have a larger capture range than traditional snakes, initialization of the contour is still critical to successful segmentation. In this study, to relax the initialization constraint, we use a coarse-to-fine approach. A

Gaussian pyramid [13] was constructed for the input image, and then the snake algorithm was applied level by level, interpolating the result of one level as the initial contour at the next lower level. Each level represents the same image with 1.5 times lower resolution in both the lateral and vertical directions. Neighboring pixels in an upper lever image are more independent because subsampling reduces their correlation. To achieve automatic segmentation, template matching at a coarse level of the Gaussian pyramid was performed first to determine an initial contour for the snake. Template matching on the low-resolution image is fast and relatively immune to noise. Since we have prior knowledge that the thermal coagulation is spherical or ellipsoidal in shape, a circular disk with a ring is used as the template. The goal is to find a dark region on a light background. The best matching position is defined where the normalized cross-correlation is maximum. A fast algorithm based on the FFT is used for template matching.

For 3D segmentation, because the spatial resolution is anisotropic, simple extension of 2D active contours to 3D active surfaces will not provide a good result. Simple interpolation in the elevational direction may introduce artifacts. Since 3D data are essentially reconstructed from 2D slices, the 2D algorithm proposed above can be applied repeatedly on the sequence of 2D images. We first apply the 2D algorithm on the central plane of the 3D data, and then we apply the algorithm to its adjacent planes. The initial lesion location and geometry on the current plane may be estimated from the processed adjacent plane.

III. RESULTS

Figure 2 is a typical automated segmentation result for a 3D data set. Only every other slice is shown. The parameters used for the algorithm were chosen by applying the algorithm on 8 thermal coagulations. This set of parameters was then used for the remaining 36 coagulations.

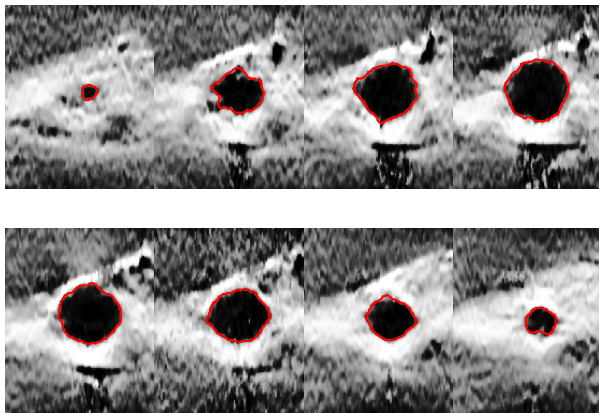


Figure 2. Segmentation of thermal coagulation on a 3D elastographic data set. Red contours are the segmentation results.

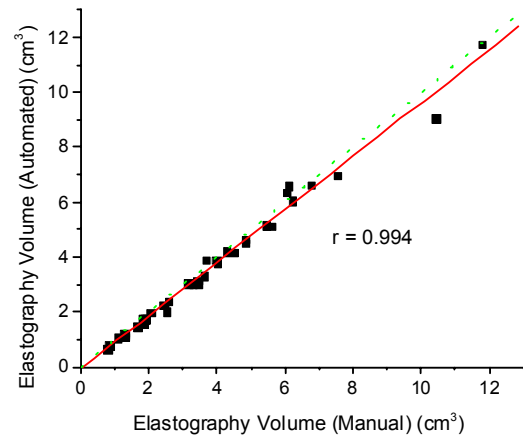


Figure 3. Coagulation volumes obtained by manual depiction versus automated segmentation. The solid line is from the least-squares fit; the dotted line is the line of equal size.

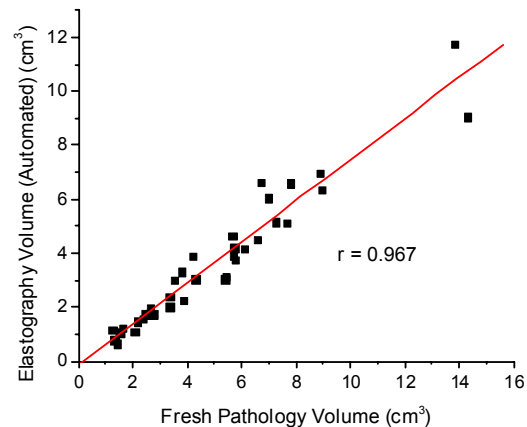
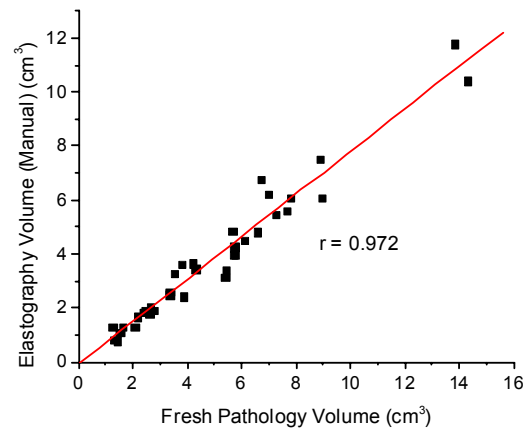


Figure 4. Coagulation volume measurements comparing manual (top) and automated (bottom) elastography volumes with volumes obtained from fixed tissue pathology.

To evaluate the segmentation result, the overlap between manual segmentation and automated segmentation is defined as: $overlap = (Manual \cap Automated) / (Manual \cup Automated)$, where \cap and \cup represent intersection and union, respectively. Based on 36 thermal coagulations, the average area overlap of the central slice elastograms was 89.5%. Using results for every image plane, average volume overlap of the segmented coagulations was 84.3%. Figure 3 shows a scatter plot of coagulation volume measurements, comparing manually delineated volumes with the automatically segmented volumes. They are highly correlated (correlation coefficient, $r = 0.994$), indicating that the automatically segmented results are very good if we assume manual depiction is the standard. Figure 4 displays scatter plots of coagulation volume measurements comparing manual or automated elastography volumes with fixed tissue pathology (manually depicted by a medical physicist). The correlation coefficient between manually delineated elastography volumes and pathology volumes is 0.972, while that between automated elastography volumes and pathology volumes is 0.967. Elastography tends to slightly underestimate the actual coagulation size found on gross pathology.

IV. DISCUSSION AND CONCLUSION

Although the results presented are for automated segmentation of *in vitro* ablation specimens, similar results are expected under *in vivo* conditions. This is due to the close correspondence between the manual and automated segmentation results. To prove this, *in vivo* elastograms for thermal coagulations in pig liver were used to test the algorithm. Only 2D images were acquired at this time. However, the results are promising as shown in Figure 5.

The close correspondence between the manual and automated segmentation results demonstrates the automated algorithm is able to provide quantitative thermal coagulation segmentations, comparable to those obtained with manual delineation.

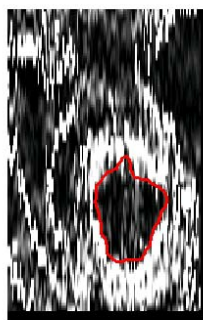


Figure 5. Automated segmentation of thermal coagulation created in pig liver *in vivo*.

- [1] S. N. Goldberg, G. S. Gazelle, and P. R. Mueller, "Thermal ablation therapy for focal malignancy: a unified approach to underlying principles, techniques, and diagnostic imaging guidance," *AJR Am J Roentgenol*, vol. 174, pp. 323-31, 2000.
- [2] S. N. Goldberg, J. W. Charboneau, G. D. Dodd, 3rd, D. E. Dupuy, D. A. Gervais, A. R. Gillams, R. A. Kane, F. T. Lee, Jr., T. Livraghi, J. P. McGahan, H. Rhim, S. G. Silverman, L. Solbiati, T. J. Vogl, and B. J. Wood, "Image-guided tumor ablation: proposal for standardization of terms and reporting criteria," *Radiology*, vol. 228, pp. 335-45, 2003.
- [3] J. T. De Sanctis, S. N. Goldberg, and P. R. Mueller, "Percutaneous treatment of hepatic neoplasms: A review of current techniques," *Cardiovasc Intervent Radiol*, vol. 21, pp. 273-96, 1998.
- [4] T. Varghese, J. Ophir, E. Konofagou, F. Kallel, and R. Righetti, "Tradeoffs in elastographic imaging," *Ultrason Imaging*, vol. 23, pp. 216-48, 2001.
- [5] J. Ophir, I. Cespedes, H. Ponnekanti, Y. Yazdi, and X. Li, "Elastography: a quantitative method for imaging the elasticity of biological tissues," *Ultrason Imaging*, vol. 13, pp. 111-34, 1991.
- [6] F. Kallel, J. Ophir, K. Magee, and T. Krouskop, "Elastographic imaging of low-contrast elastic modulus distributions in tissue," *Ultrasound Med Biol*, vol. 24, pp. 409-25, 1998.
- [7] A. Fenster, D. B. Downey, and H. N. Cardinal, "Three-dimensional ultrasound imaging," *Phys Med Biol*, vol. 46, pp. R67-99, 2001.
- [8] T. Varghese, J. A. Zagzebski, and F. T. Lee, Jr., "Elastographic imaging of thermal lesions in the liver *in vivo* following radiofrequency ablation: preliminary results," *Ultrasound Med Biol*, vol. 28, pp. 1467-73, 2002.
- [9] T. Varghese and H. Shi, "Elastographic imaging of thermal lesions in liver *in-vivo* using diaphragmatic stimuli," *Ultrason Imaging*, vol. 26, pp. 18-28, 2004.
- [10] W. Liu, U. Techavipoo, T. Varghese, J. A. Zagzebski, Q. Chen, and F. T. Lee, Jr., "Elastographic versus x-ray CT imaging of radio frequency ablation coagulations: an *in vitro* study," *Med Phys*, vol. 31, pp. 1322-32, 2004.
- [11] R. Righetti, F. Kallel, R. J. Stafford, R. E. Price, T. A. Krouskop, J. D. Hazle, and J. Ophir, "Elastographic characterization of HIFU-induced lesions in canine livers," *Ultrasound Med Biol*, vol. 25, pp. 1099-113, 1999.
- [12] U. Techavipoo, T. Varghese, J. A. Zagzebski, Q. Chen, and W. Liu, "Semiautomated thermal lesion segmentation for three-dimensional elastographic imaging," *Ultrasound Med Biol*, vol. 30, pp. 655-64, 2004.
- [13] P. Burt and E. H. Adelson, "A Multiresolution Spline With Application to Image Mosaics," *ACM Trans. Graphics*, vol. 2, pp. 217-236, 1983.
- [14] C. Xu and J. L. Prince, "Snake, shapes, and gradient vector flow," *IEEE Trans Image Processing*, vol. 7, pp. 359 - 69, 1998.
- [15] F. Kallel and J. Ophir, "A least-squares strain estimator for elastography," *Ultrason Imaging*, vol. 19, pp. 195-208, 1997.
- [16] T. Cootes, A. Hill, C. J. Taylor, and J. Haslam, "Use of Active Models for Locating Structure in Medical Images," *Image and Vision Computing*, vol. 12, pp. 355-365, 1994.
- [17] M. Kass, A. Witkin, and D. Terzopoulos, "Snakes: Active Contour Models," *International Journal of Computer Vision*, vol. 1, pp. 321-331, 1987.